Turbulent Static Pressure Fluctuations Away from Flow Boundaries

N. M. Komerath,* U. G. Hegde,† and W. C. Strahle‡
Georgia Institute of Technology, Atlanta, Georgia

A technique for measuring static pressure fluctuations and the pressure-velocity correlation away from walls in interior and exterior turbulent flows is described. Direct response calibration using Fourier transform techniques enables the use of a microphone pitot probe and a hot-film sensor to derive the static pressure spectrum. Experiments verifying the assumptions made in using this technique are described. Theoretical computations are made that show excellent agreement with the measured values. The pressure fluctuations away from walls are seen to be much larger than those sensed by wall-mounted transducers.

Nomenclature

a = pipe radius
A_{u_1} = velocity sensitivity of hot film probe in $ms^{-1}V^{-1}$
a_1, a_2 = quantities defined by Eq. (17)
f = frequency
h = distance from pipe wall
l_{cor} = integral length scale for velocity fluctuations
M = microphone probe signal
P = static pressure
P_T = total pressure
r = radial distance
S = spectral density
t = time
u = incompressible part of velocity vector
v = velocity vector
v_a = acoustic part of velocity vector
x = axial distance
γ = cross-correlation coefficient
θ = angle
μ = absolute viscosity
ρ = density
ω = radian frequency

Subscripts

H = hot-film probe signal
i = axial and radial components, = 1,2
r = raw signal, uncorrected for response
ω = Fourier transform

Superscripts

$( )'$ = fluctuations
$( )^*$ = complex conjugate
$\overline{( )}$ = ensemble average

Introduction

STATIC pressure fluctuations in interior and exterior flows, away from flow boundaries, are important in aeroacoustics and in turbulent flow descriptions. In aeroacoustics, the static pressure is of interest insofar as radiated noise is concerned, and in turbulent flows, the correlation between pressure and velocity is important in the determination of stress transport. Not widely recognized, but of great technical significance, is the fact that pressure fluctuations away from, but near, flow boundaries can differ substantially from wall-measured values. This phenomenon is investigated herein for a particular flow, and correlations between pressure and velocity fluctuations are also obtained.

The lack of reliable methods has severely hampered the measurement, and, hence, understanding, of turbulent static pressure fluctuations away from flow boundaries. The most widely accepted method for measuring pressure has been to locate sensing holes on surfaces aligned with the mean flow direction. In subsonic flows, if the sensing location is sufficiently far downstream of the leading edge or nose of the probe, the static pressure in the freestream is recovered. When such probes are used in turbulent flows to measure pressure fluctuations, several problems are encountered. Static pressure probes are inherently sensitive to three-dimensional fluctuations in angle of attack. Furthermore, fluctuations sensed on a probe surface tangential to the mean flow direction may not differ from those sensed on other flow boundaries and, hence, may not reveal the phenomenon investigated here.

Presented herein is a method to extract static pressure fluctuations from the fluctuations sensed at the tip of a pitot tube. It is well established that a pitot tube measures the total pressure reliably even in moderately turbulent flows,[1,2] being quite insensitive to components of velocity normal to its axis, as well as to minor variations in probe geometry. The relation between instantaneous total and static pressure is simple, especially in constant-density flows. Under the assumption of quasisteady flow, simultaneous knowledge of the total pressure, velocity, and density in the freestream enables time-resolved calculation of static pressure.

Bryer and Pankhurst[2] have reviewed the problems encountered in the use of a microphone pitot tube to get time-resolved measurements. Basically, these problems stem from the need to account for the effects of the tube separating the transducer from the measuring location. The resonant frequencies of the system are functions of the length of the tube and the width of the air gap in front of the microphone diaphragm. The signal obtained with the probe is generally dominated by the resonant frequencies unless the system is critically damped, in which case the signal-to-noise ratio suffers. By careful construction, the resonances can be shifted to higher frequencies. By trial and error, critical damping can be used by means of soft material stuffed into the tube to obtain an approximately flat frequency response curve over most of the frequency range of interest. However, this still leaves the phase lag characteristics of the system uncorrected, and the large errors introduced by these

Received June 15, 1983; revision received Dec. 13, 1984.

*Post Doctoral Fellow. Member AIAA.
†Graduate Research Assistant. Student Member AIAA.
‡Regents' Professor. Associate Fellow AIAA.

characteristics make simultaneous measurements with other probes difficult. For these reasons, the microphone pitot probe has not been used widely except to obtain rms values. A method for direct determination of the complex frequency response function, and of compensation, is described in later paragraphs.

Principle of Measurement

In a steady incompressible flow, the pressure at the tip of a pitot probe is

$$P_T = P + \tfrac{1}{2}\rho u_1^2 \tag{1}$$

When the probe tip is in a turbulent stream, the pressure at the probe tip fluctuates. Decomposition of Eq. (1) gives

$$P_T' = P' + \tfrac{1}{2}[\bar{\rho}(u_1'^2 - \overline{u_1'^2}) + 2\bar{\rho}\bar{u}_1 u_1' + \rho' \bar{u}_1^2 + (\rho' u_1'^2 - \overline{\rho' u_1'^2}) + 2(\rho' u_1' \bar{u}_1 - \rho' u_1' \bar{u}_1)] \tag{2}$$

Use of this equation for measurement of P' assumes the following:

1) The instantaneous pressure is uniform over the opening at the probe tip.

2) Pressure fluctuations due to cross-flow velocity fluctuations are negligible.

3) Deceleration to zero velocity is isentropic and quasisteady, and occurs over a distance of a few probe diameters upstream.

4) P' is of the same order of magnitude as the largest of the other terms.

5) The presence of the probe does not cause large fluctuations in the flow around and ahead of its tip.

In an isothermal, incompressible flow of a single perfect gas, Eq. (2) reduces to

$$P_T' \approx P' + \bar{\rho}\bar{u}_1 u_1' \tag{3}$$

In turbulent jets, and away from the walls in turbulent pipe flows, most of the kinetic energy of turbulence is known to be contained in the large-scale eddies. In flows where the integral scale of the velocity fluctuations is considerably larger than the probe tip, assumption 1 is reasonable. Also, a velocity sensor can be located in the undisturbed stream near the pitot tip to measure the velocity sensed by the pitot probe with good accuracy. For low Mach number flows, isentropic deceleration is a valid assumption. The other assumptions can be verified experimentally, as described subsequently.

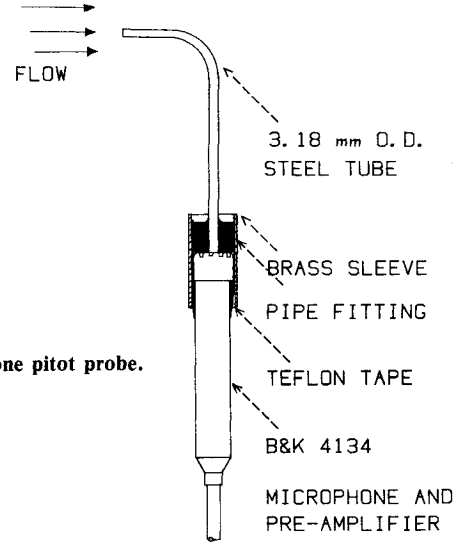

Fig. 1 Microphone pitot probe.

Construction

A microphone pitot probe is shown in Fig. 1. It consists of a steel tube bent through 90 deg, with one end fixed inside a hollow pipe fitting. A B&K 4134 12.5-mm condenser microphone is pressed against the pipe fitting and sealed pressure-tight using teflon tape and a brass sleeve. This construction allows equalization of pressure on both sides of the diaphragm without allowing mean flow through the pitot tube. The protective grid in front of the diaphragm makes the probe simple and rugged, and allows the use of tubes of much smaller diameter than the diaphragm. A B&K Type 2615 preamplifier and power supply complete the data acquisition system.

Calibration and Response Compensation

The microphone and preamplifier were calibrated by the manufacturers and showed flat frequency response to over 20 kHz as well as a sensitivity of 11 mV/N/m^2. The phase angle between incident pressure and output voltage was 180 deg at low frequencies, falling to 177 deg by 2.5 kHz. The sensitivity of a reference microphone of the same type was checked using a B&K calibrator and was found to match the manufacturer's calibration values. Thus, the sensitivity and response of a reference system to pressure were determined.

The probe microphone, removed from the probe, was placed close to the reference microphone, in front of a source of broadband acoustic pressure fluctuations. The preamplified signals from the two microphones were fed through low-pass filters into a Hewlett Packard Fourier analyzer. The autopower spectra, coherence function, and transfer function of the two signals were computed. The spectra were identical, and the coherence function and magnitude of the transfer function were close to unity. The phase was negligibly small. This demonstrated the close similarity between the two microphones, and that the sound

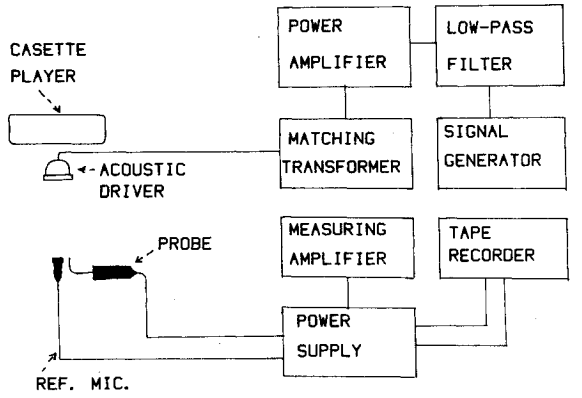

Fig. 2 Determination of microphone probe frequency response.

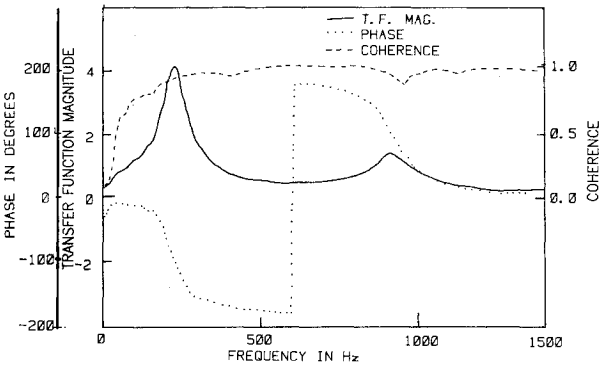

Fig. 3 Transfer function and coherence for a 3-mm-o.d. microphone pitot probe.

field was of the same amplitude and phase at their sensing elements at the same time.

With the probe microphone inside the probe, and the pitot tip close to the reference microphone, the procedure was repeated as shown in Fig. 2. The transfer function was recorded in digital form and used to correct incoming data samples. A typical raw transfer function and the corresponding coherence function are shown in Fig. 3.

The transfer function for a given probe was quite repeatable. However, recalibration was performed whenever the probe was reassembled or subjected to rough handling.

The sound sources used in the calibration setup produced very little sound below 100 Hz. This resulted in the signal-to-noise ratio and, hence, the coherence being low in the first few channels of the digitized transfer function. Linear interpolation, starting from the known zero-frequency value of $1+i0$ (for identical microphones) was used to correct the transfer function up to the point where the coherence function exceeded 0.75. This involved frequencies from 15 to 120 Hz. It should be noted that the transfer function was low only because of poor signal-to-noise ratio during calibration. The shape of the magnitude and phase plots indicates that linear interpolation in this range is quite satisfactory. In the turbulent flow investigated, the signal is quite strong at the low frequencies, and, hence, no problems are encountered.

Testing

The calibration procedure was repeated for varying values of the separation between the probe tip and reference microphones. The transfer function proved to be independent of small variations in the calibration setup. The sensitivity of the probe to external noise was checked with the probe tip closed, and found to be negligible. The probe was leak-tested to over 3×10^5 N-m^2 air pressure at the tip.

Initial experiments were conducted in a cold jet to check signal level and the adequacy of the response correction. The uncorrected spectra showed peaks at the resonance frequencies, which disappeared after response correction, leaving autospectra whose shapes indicated an energy distribution similar to that in the velocity spectrum. Transfer functions evaluated when the calibration signal was around 100 dB were used successfully to correct spectra obtained in flows where the signal level was up to 138 dB, showing that the assumptions of linear sensitivity to pressure, and of a linear transfer function, are justified.

A probe with a 1-mm o.d. was placed close to the tip of the 3-mm-o.d. probe in a cold jet to study the error due to the quasisteady assumption. This error was expected to cause a phase shift between the two signals, increasing linearly with frequency, since the probes differed in diameter by a factor of 3. Figure 4 shows the comparison between the signals. The phase difference is seen to be quite small below 1250 Hz, beyond which the signal measured by the smaller probe was unreliable.

Cross-flow error was checked by wrapping a strip of fine-meshed platinum gauze around the tip of the 1-mm probe, thus obstructing cross-flow fluctuations without affecting axial velocity fluctuations. No change was observed in the autospectrum of the signal.

The influence of the probe on upstream flow was checked by traversing a 50-μm hot-film sensor axially in front of the 3-mm probe in the core region of fully developed turbulent pipe flow. The results, shown in Fig. 5, verify the assumption that the deceleration occurs within 7-10 mm, equivalent to 2-3 probe diameters.

The accuracy of computation of pressures in a turbulent pipe flow was tested using an acoustic source. A driver was located in the wall of the pipe, upstream of the axial location of the 3-mm probe, a hot film, and a wall-mounted microphone. When the driver was excited at a discrete frequency, the resulting pressure fluctuations were predominantly of a plane-wave nature, so that both the wall microphone and probe tip were expected to experience the same pressure fluctuations. As shown in Fig. 6, results agreed well over a wide range of frequencies. This shows that the probe does sense static pressure fluctuations accurately in a turbulent flowfield, that it does not induce large pressure fluctuations at its tip, and that the data-reduction procedure is adequately accurate.

The assumption that the pressure fluctuations are of the same order of magnitude as $\rho\bar{u}_1u_1'$ was tested by examining the cross spectrum between velocity fluctuations, obtained with a hot-film probe, and total pressure fluctuations obtained with the microphone pitot probe, in the core region of a turbulent pipe flow. A typical cross-spectrum plot is shown in Fig. 7. If P_T were dominated by the term $\overline{\rho u_1 u_1'}$, one would expect these two quantities to have zero phase relative to each other. The large phase angle of about 50 deg, at low frequencies, can only be explained by concluding that static pressure fluctuations, which are later shown to be nearly 180 deg out of phase with velocity fluctuations, are, in fact, of the same order of magnitude as $\rho\bar{u}_1u_1'$.

Interference effects on other probes due to the microphone probe were tested by comparing the spectra obtained from the 1-mm probe, with and without the 3-mm probe in its vicinity. No difference was noticeable. The data-reduction scheme was checked for any case of accumulation of round-off or truncation error. Results obtained proved to be repeatable.

Investigation of Cold Turbulent Pipe Flow

The experimental setup is shown in Fig. 8. Fully developed, turbulent pipe flow was created by connecting a long 2-in.-diam PVC pipe to a bellmouth inlet at one end and a convergent-divergent nozzle at the other, the nozzle

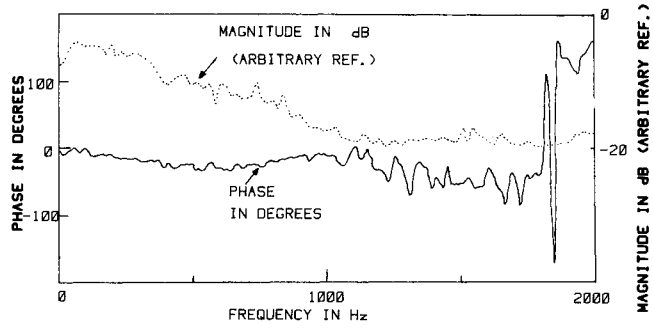

Fig. 4 Cross spectrum between two microphone probes with different tip diameters.

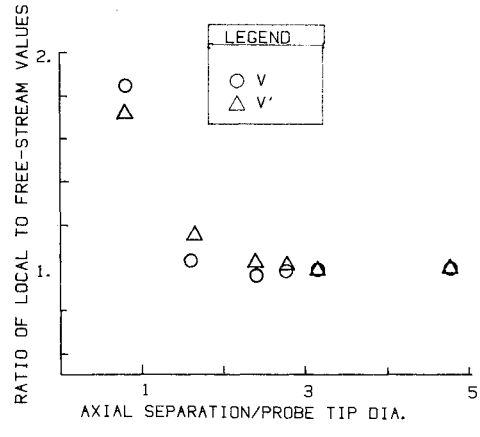

Fig. 5 Ratios of mean and rms velocities measured ahead of a 3-mm microphone probe to freestream values.

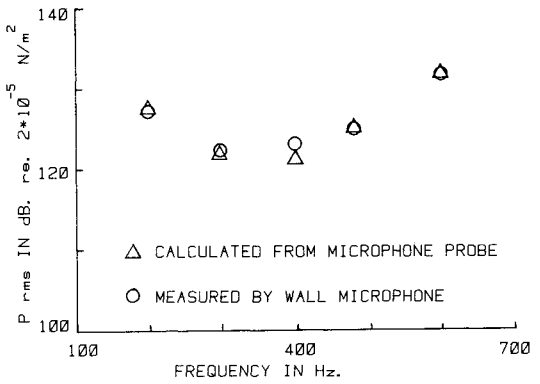

Fig. 6 Comparison of pressure fluctuations measured with a wall microphone and 3-mm microphone probe at the frequency of an acoustic driver.

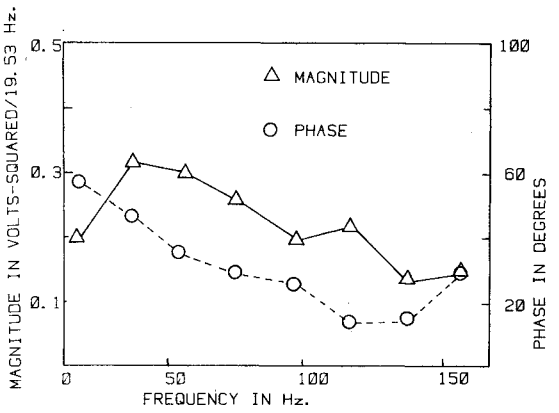

Fig. 7 Low-frequency content of cross spectrum between total pressure and velocity in cold-pipe flow.

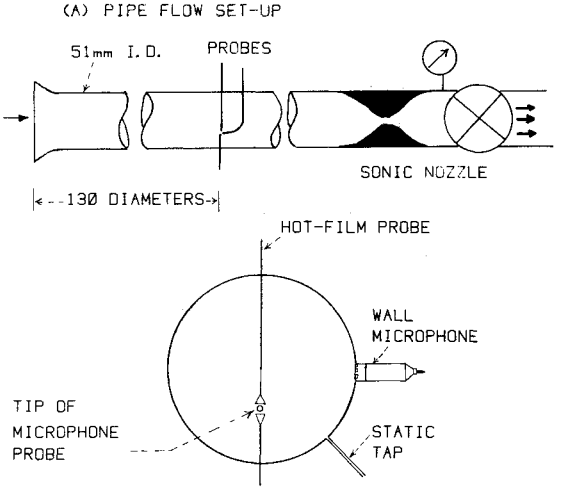

Fig. 8 Cold-pipe flow facility and probe configuration.

exit being connected through a valve to a large vacuum tank. Opening the valve caused the nozzle throat to become sonic, ensuring that flow noise from downstream of the throat would not propagate upstream. A short section of the pipe, more than 100 diameters downstream of the bellmouth inlet, was used as the test section, and fitted with ports for various probes.

The test section was instrumented as shown in Fig. 8, with the microphone probe, hot-film probes, a flush-mounted

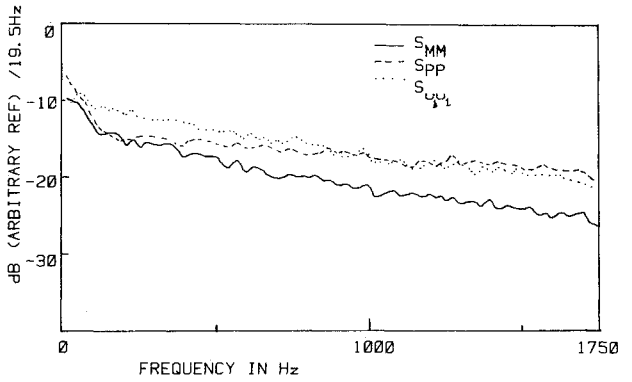

Fig. 9 Autospectral densities of total pressure, velocity, and static pressure at $r = a/2$ in cold-pipe flow.

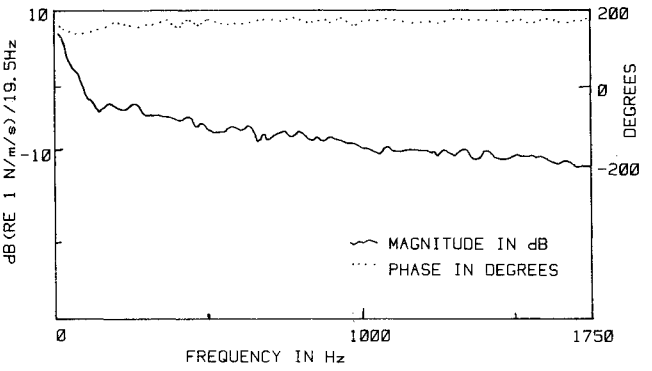

Fig. 10 Cross spectrum between static pressure and velocity.

wall microphone, and a wall static pressure tapping. Anemometer signals were monitored on digital voltmeters and oscilloscopes, and the fluctuating signal obtained after filtering out the mean value was amplified and recorded on magnetic tape. The preamplified microphone signals were also recorded on tape simultaneously. The mean wall static pressure was measured using a Barocel transducer.

Data Analysis

The fluctuating voltage signals $M_r(t)$ and $E_H(t)$ from the microphone probe and hot-film anemometer, respectively, were sampled by the analog-to-digital converter of the Fourier analyzer. Fourier transforms $M_{r\omega}$ and $E_{H\omega}$ were computed. The hot-film velocity sensitivity A_{u_1} and the microphone probe transfer function $H(f)$ were used to convert the sample Fourier transforms to transforms of the velocity and total pressure, respectively. Thus,

$$u_{1\omega} = E_{H\omega}/A_{u_1} \tag{4}$$

and

$$M_\omega = M_{r\omega}/H(f) = P_\omega + B_{u_1} u_{1_\omega} \tag{5}$$

where

$$A_{u_1} = 1/2\bar{E}_H \bar{u}_1^{0.55} \quad \text{and} \quad B_{u_1} = \rho \bar{u}_1 \tag{6}$$

Auto- and cross spectra were computed from the transforms $E_{H\omega}$ and M_ω, and ensemble averaged over 100 samples. From Eqs. (4) and (5),

$$S_{u_1u_1} = S_{HH}/A_{u_1}^2 \tag{7}$$

$$S_{Pu_1} = (S_{MH} - A_{u_1} B_{u_1} S_{u_1u_1})/A_{u_1} \tag{8}$$

$$S_{PP} = S_{MM} - B_{u_1}^2 S_{u_1u_1} - 2B_{u_1} \mathrm{Re}(S_{u_1P}) \tag{9}$$

The mean square pressure fluctuation was determined by integrating S_{PP}, and the pressure-velocity correlation was obtained by taking the inverse Fourier transform of S_{u_1P}. The cross-correlation coefficient was obtained as

$$\gamma_{uP}=\frac{F^{-1}(S_{u_1P})}{[F^{-1}(S_{u_1u_1})F^{-1}(S_{PP})]^{0.5}} \tag{10}$$

Experimental Results

Autospectra of the total pressure, velocity, and static pressure at the half-radius position of the pipe are presented in Fig. 9. The cross-spectrum between total pressure and velocity is shown in Fig. 7. The cross spectrum between pressure and velocity is shown in Fig. 10, and the cross-correlation function in Fig. 11.

The spectra of total pressure, velocity, and static pressure were found to follow the same shape, falling off as frequency increased. The phase angle between pressure and velocity was nearly 180 deg over the entire frequency range, indicating a direct causal relationship. The pressure-velocity correlation and the correlation coefficient are plotted in Fig. 12. The correlation is negative, with the coefficient between -0.5 and -0.7, indicating that, most of the time, when the pressure increased, the velocity decreased, and vice versa.

The rms of the pressure fluctuation was on the order of 130 dB re 2×10^{-5} N/m^2. These values did not change much along the pipe radius, as shown in Fig. 13. Measurements close to the wall are difficult to make with the system used here since the assumption of large velocity scales and slow spatial variations may break down in regions of steep velocity gradient, and also because the probe diameter is larger than the thickness of the wall layer where velocity goes to zero. As far as could be measured, the rms pressure showed a minimum at the pipe axis, increasing slightly toward the wall. The level measured at the wall, however, is 113 dB. This large difference posed a difficult paradox until it was explained through analytical computation, as described below.

Analysis

To obtain a theoretical estimate of the fluctuating static pressure in fully developed pipe flow, the momentum equation along the axial direction is considered.

$$\rho\frac{Dv_1}{Dt}=-\frac{\partial P}{\partial x}+\mu\nabla^2u_1+\frac{1}{3}\mu\frac{\partial}{\partial x}(\nabla\cdot v) \tag{11}$$

The velocity v is split into its incompressible and acoustic components $v=u+v_a$ with $\nabla\cdot u=0$. In the core flow effects of viscosity are negligible. Also acoustic velocities may be neglected compared to velocities associated with the incompressible field. Then in the core flow Eq. (11) becomes

$$\rho\left[\frac{\partial u_1}{\partial t}+(u\cdot\nabla)u_1\right]=-\frac{\partial P}{\partial x}$$

Linearizing with respect to the fluctuating turbulent velocities yields the linearized momentum equation for fluctuating quantities

$$\frac{\partial P'}{\partial x}=-\rho\left[\frac{\partial u_1'}{\partial t}+\bar{u}_1\frac{\partial u_1'}{\partial x}+u_2'\frac{d\bar{u}_1}{dr}\right] \tag{12}$$

where u_2' is the fluctuation in the radial component of the incompressible velocity u.

Taking the Fourier transform of Eq. (2) and integrating between $x=x_1$ and x_2 yields

$$-\frac{1}{\rho}[P_\omega(x_2)-P_\omega(x_1)]=i\omega\int_{x_1}^{x_2}u_{1\omega}(x_0)dx_0$$
$$+\bar{u}_1[u_{1\omega}(x_2)-u_{1\omega}(x_1)]+\frac{d\bar{u}_1}{dr}\int_{x_1}^{x_2}u_{2\omega}(x_0)dx_0$$

On multiplying the above equation by its conjugate and taking an ensemble average,

$$\frac{1}{\rho^2}[\overline{P_\omega^*(x_2)P_\omega(x_2)}+\overline{P_\omega^*(x_1)P_\omega(x_1)}-\overline{P_\omega^*(x_2)P_\omega(x_1)}$$
$$-\overline{P_\omega^*(x_1)P_\omega(x_2)}]=\omega^2\int_{x_1}^{x_2}\int_{x_1}^{x_2}\overline{u_{1\omega}^*(\tilde{x})u_{1\omega}(x_0)}dx_0d\tilde{x}$$
$$+\left(\frac{d\bar{u}_1}{dr}\right)^2\int_{x_1}^{x_2}\int_{x_1}^{x_2}\overline{u_{2\omega}^*(\tilde{x})u_{2\omega}(x_0)}dx_0d\tilde{x}$$
$$+\bar{u}_1^2[\overline{u_{1\omega}^*(x_2)u_{1\omega}(x_2)}+\overline{u_{1\omega}^*(x_1)u_{1\omega}(x_1)}-\overline{u_{1\omega}^*(x_2)u_{1\omega}(x_1)}$$
$$-\overline{u_{1\omega}^*(x_1)u_{1\omega}(x_2)}]-2\omega\frac{d\bar{u}_1}{dr}\mathrm{Im}\int_{x_1}^{x_2}\int_{x_1}^{x_2}\overline{u_{2\omega}^*(\tilde{x})u_{1\omega}(x_0)}dx_0d\tilde{x}$$
$$+2\omega\bar{u}_1\mathrm{Im}\int_{x_1}^{x_2}[\overline{u_{1\omega}(x_0)u_{1\omega}^*(x_1)}-\overline{u_{1\omega}(x_0)u_{1\omega}^*(x_2)}]dx_0$$
$$+2\bar{u}_1\frac{d\bar{u}_1}{dr}\mathrm{Re}\int_{x_1}^{x_2}[\overline{u_{2\omega}^*(x_0)u_{1\omega}(x_2)}-\overline{u_{2\omega}^*(x_0)u_{1\omega}(x_1)}]dx_0 \tag{13}$$

In general, Eq. (13) would need a detailed knowledge of the various correlations to be useful. However, taking (x_2-x_1) to be on the order of an integral length scale l_{cor} and assuming that quantities are perfectly correlated in this interval and uncorrelated outside of it the equation becomes tractable. On simplifying

$$\frac{2}{\rho^2}\overline{P_\omega^*(x)P_\omega(x)}\approx\omega^2(l_{cor})^2\overline{u_{1\omega}^*u_{1\omega}}$$
$$+\left(\frac{d\bar{u}_1}{dr}\right)^2(l_{cor})^2\overline{u_{2\omega}^*u_{2\omega}}+2\bar{u}_1^2\overline{u_{1\omega}^*u_{1\omega}}$$

Now $\overline{u_{1\omega}^*u_{1\omega}}$ and $\overline{u_{2\omega}^*u_{2\omega}}$ are of the same order of magnitude so that the relative importance of the terms on the right-hand side is determined by comparing

$$\omega^2(l_{cor})^2,\qquad\left(\frac{d\bar{u}_1}{dr}\right)^2(l_{cor})^2$$

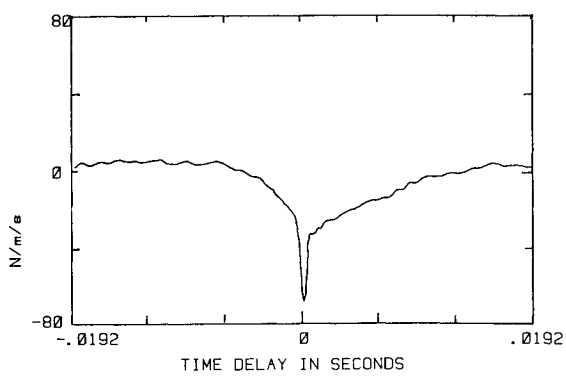

Fig. 11 Cross-correlation function between pressure and velocity.

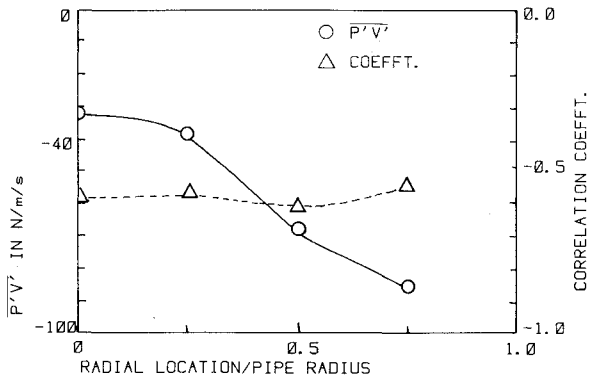

Fig. 12 The p-v correlation and correlation coefficient along the pipe radius.

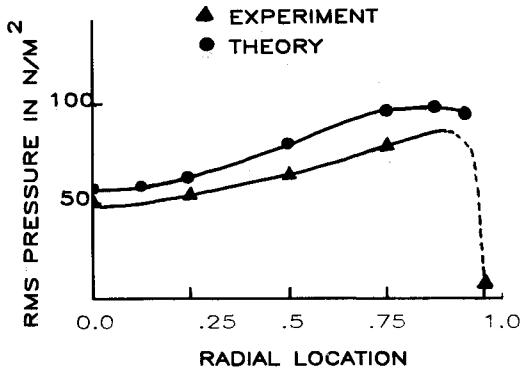

Fig. 13 Comparison of theoretical and experimental values of rms pressure.

and $2\bar{u}_1^2$ in the core flow. Typical values of frequency and the associated length scale are 400 Hz and 0.007 m. A typical $d\bar{u}_1/dr$ in the core flow is 500/s and the velocity is on the order of 40 m/s. The dominant term is then seen to be $2\bar{u}_1^2\overline{u_{1\omega}^* u_{1\omega}}$. Thus, in the core flow

$$\overline{P_\omega^*(x)P_\omega(x)} \approx \rho^2 \bar{u}_1^2 \overline{u_{1_\omega}^* u_{1_\omega}} \tag{14}$$

implying that the frequency content of the pressure fluctuations closely matches the frequency content of the fluctuating axial velocity.

On summing Eq. (14) over all frequencies,

$$\overline{P'^2} \approx \rho^2 \bar{u}_1^2 \overline{u_1'^2} \tag{15}$$

which relates the mean square fluctuating pressure to the mean square fluctuating axial velocity.

To discern what occurs in the wall region, Eq. (11) is considered along the wall at $r=a$. On the walls, v vanishes and the pressure gradient is balanced by the viscous terms. The momentum equation for fluctuating quantities along the wall becomes

$$\frac{\partial P'}{\partial x} = \mu\left[\nabla^2 u_1' + \frac{1}{3}\mu\frac{\partial}{\partial x}(\nabla\cdot v_a) + \mu\nabla^2 v_{a_1}\right] \tag{16}$$

The purpose is to compare the pressure fluctuations at the walls to those in the interior. Toward this end, only an order of magnitude for the pressure fluctuations at the wall will be sought.

To this end, the first term on the right-hand side of Eq. (16) is considered. Following Ref. 3, u_1' in the wall region is expressed as a series in h, the distance from the wall.

$$u_1'(x,h,\theta,t) = a_1(x,\theta,t)h + a_2(x,\theta,t)h^2 + \ldots \tag{17}$$

Then, at $r=a(h=0)$,

$$\nabla^2 u_1' = 2a_2 - (a_1/a)$$

Since experimental values of a_1 are available,[3] the effect of a_1 alone will be considered. Following the procedure used in the core flow

$$\overline{P_\omega^*(x)P_\omega(x)} \sim (2\mu/a^2)\overline{a_{1\omega}^* a_{1\omega}}(l_{\text{cor}})_{\text{wall}}^2 \tag{18}$$

where $(l_{\text{cor}})_{\text{wall}}$ is an integral length scale for a_1 at the wall. Summing over all frequencies an estimate for the mean square pressure at the wall is obtained.

$$\overline{P_{\text{wall}}'^2} \sim (2\mu^2/a^2)\overline{a_1^2}(l_{\text{cor}})_{\text{wall}}^2 \tag{19}$$

Comparing the pressure level at the wall to that in the interior

$$\frac{\overline{P'^2})_{\text{wall}}}{\overline{P'^2})_{\text{interior}}} \sim \frac{(2\mu^2/a^2)\overline{a_1^2}(l_{\text{cor}})^2_{\text{wall}}}{\rho^2 \bar{u}_1^2 \overline{u_1'^2}}$$

The value of $\overline{a_1^2}$ is obtained from Ref. 3. Substituting the appropriate values for the other quantities,

$$\frac{\overline{P'^2})_{\text{wall}}}{\overline{P'^2})_{\text{interior}}} \sim 10^{-4}(l_{\text{cor}})^2_{\text{wall}} a^{-2} \tag{20}$$

An upper limit to the $(l_{\text{cor}})_{\text{wall}}$ is most certainly the tube radius which, in the experimental case considered, is 0.0254 m. Therefore, it is clear that the pressure level at the wall is at least an order of magnitude lower than that in the core flow.

The transverse variation of the pressure fluctuations may now be understood. The behavior of the fluctuating pressure level in the core flow is the behavior of $\bar{u}_1\sqrt{\overline{u_1'^2}}$. It has a local minimum on the tube centerline and then increases with radial distance until its maximum value is reached close to the wall. According to Eq. (20), the pressure level at the wall is much lower than in the core flow. Thus, it is expected that the pressure level increases with radial coordinate, reaches a maximum, and then drops substantially. The fluctuation level computed using Eqs. (15) and (20) is compared to the measured level in Fig. 13, and shows good agreement.

Conclusions

1) A technique has been developed to deduce turbulent static pressure fluctuations from simultaneous measurements of impact pressure and velocity in turbulent flows of low Mach number.

2) A method has been demonstrated for performing dynamic calibration and compensation of the frequency response of a microphone pitot probe.

3) It has been shown that the assumption of quasi-steadiness can be used, with negligible error, in interpreting impact probe spectra, at least with the apparatus used.

4) Cross-flow fluctuations are seen to have very little effect on the pressure sensed by square-nosed impact pressure probes.

5) The new technique has been used to study the pressure fluctuations in the interior of a fully developed turbulent pipe flow, and the results show that these fluctuations are much larger than those sensed by wall-mounted transducers.

6) The spectrum of turbulent pressure fluctuations in pipe flow is broadband, and resembles that of the velocity fluctuations.

7) Acoustic pressures are seen to be faithfully impressed upon the wall, however, in the freestream, the fluctuations in the pressure field carried by the vortical flow are much larger than the acoustic fluctuations.

8) The cross correlation between the pressure and velocity fluctuations is negative, with their phase difference being close to 180 deg over the entire frequency range studied. The correlation coefficient attains high values.

9) Theoretical computations support and explain the observed phenomena. Agreement between computed and measured pressure fluctuation levels is good.

Acknowledgment

The authors gratefully acknowledge the assistance rendered by Mr. S. B. S. Chandran in conducting many of the experiments described herein.

References

[1]Peterson, C. W. and George, O. L., "Wind Tunnel Pressure Probes: New Calibrations for New Geometries and Flow Environments," Sandia Laboratories, Albuquerque N.M., SAND-75-0337, June 1975.

[2]Bryer, D. W. and Pankhurst, R. C., *Pressure Probe Methods for Determining Wind Speed and Flow Direction*, Her Majesty's Stationery Office, London, 1971.

[3]Derksen, R. W. and Azad, R. S., "Behavior of the Turbulent Energy Equation at a Fixed Boundary," *AIAA Journal*, Vol. 19, Feb. 1981, pp. 238-239.